energies

MDPI

Article

Combustion Characterization and Heat Loss Determination Through Experimental Investigation of Hydrogen Internal Combustion Engine

Andrew Fenech [1], Stefan Portelli [1], Emiliano Pipitone [2] and Mario Farrugia [1,*]

[1] Mechanical Engineering Department, University of Malta, MSD 2080 Msida, Malta; andrew.fenech.20@um.edu.mt (A.F.); stefan.portelli.17@um.edu.mt (S.P.)
[2] Department of Engineering, University of Palermo, 90128 Palermo, Italy; emiliano.pipitone@unipa.it
* Correspondence: mario.a.farrugia@um.edu.mt

Abstract

Hydrogen combustion is known to be fast compared to traditional hydrocarbon fuels. The fast combustion leads to a higher thermal efficiency. In this research a 600 cc single cylinder hydrogen engine was tested at 1250 rpm, lambda = 2 and 3, and three load levels (load was represented by Manifold Absolute Pressure (MAP); MAPs tested were 75, 95 and 120 kPa) and compared to operation with gasoline and propane. The fast burn duration (Mass Fraction Burnt MFB10% to MFB90%) and the MFB 50% were determined and analyzed. The hydrogen MFB50% location for Minimum Timing for Best Torque (MBT) was found to occur at around the typical 8 Crank Angle Degrees (CADs) After Top Dead Center (ATDC). Measurements of ignition delay based on the fast data direct measurement of spark ignition coil current drop to the change in polarity of net heat release are presented. With shifts towards direct injection and higher injection pressures, consideration was given to the hydrogen pressurization penalty, where it was calculated that pressurizing hydrogen to 100 bar at the flow required for lambda = 2 operation is 2.3 bar, i.e., higher than the Friction Mean Effective Pressure (FMEP)! Furthermore, hydrogen is widely cited to have a higher heat loss than typical hydrocarbon fuels. In this paper, detailed analyses at lambda 2 and lambda 3 showed that hydrogen in fact has lower heat losses.

Keywords: hydrogen combustion; combustion characterization; mass burnt fraction; lean combustion

Academic Editors: Vincenzo Liso and Samuel Simon Araya

Received: 29 January 2026
Revised: 26 February 2026
Accepted: 10 March 2026
Published: 12 March 2026

1. Introduction

As early as 1939, the inventor Rudolf Arnold Erren had worked on hydrogen internal combustion engines and patented one of his hydrogen engine inventions. This engine was a single cylinder that had a valve in the cylinder wall, i.e., direct injection. Erren pointed out that, preferably, the hydrogen injection is within a 60 Crank Angle Degree (CAD) from the air inlet valve closure [1].

Recently hydrogen is being actively considered as a green fuel to reduce CO_2 generation. Furthermore, hydrogen is considered as a form of energy storage to even out excess electricity from wind and solar energy generation. Hydrogen use in internal combustion engines provides an alternative solution to fuel cells. When hydrogen is used in internal combustion engines, it makes use of existing technologies, which could be a quick solution to the widespread use of hydrogen.

As electronic engine controls have now become integral to internal combustion engines, recent interest in hydrogen internal combustion engines has benefitted from additional control features that were not possible a few decades ago. Port, or direct injection, is nowadays electronically controlled in gasoline, propane or diesel engines. Injection timing as well as injection pressure are control variables that influence performance, efficiency and emissions. In hydrogen engines, port and direct injection are both used but direct injection is used to reduce the tendency to backfire and to reduce engine derating [2,3]. Engine derating with hydrogen use is due to the fact that the hydrogen air-to-fuel ratio (by volume) is very different from typical hydrocarbon fuels. Hydrogen has a very low density compared to other fuels. Having such a low density, the hydrogen volume required for a stoichiometric mixture with air is around 1/3 of the cylinder. This effectively means that hydrogen displaces a considerable amount of air that would otherwise have entered the engine, resulting in pronounced engine derating even at lambda (λ) = 1.

While direct injection shows marked benefits, researchers sometimes in reality end up with the need to increase the Duration Of Injection (DOI) considerably to allow enough time for the flow of the required hydrogen with the consequence of the injection of hydrogen being initiated early in the intake stroke [2,4]. Researchers end up resorting to such a prolonged DOI due to the low flow capability of the used (commercially available) injectors. This renders the practical direct injection method to be port injection. Furthermore, some researchers are testing hydrogen direct injection with considerably high pressures around or above 100 bar [5–7]. These direct injection pressures are low compared to diesel injection pressures, but unlike diesel being liquid, hydrogen is a low density gas. Compression of a gas is very energy greedy, and the literature does not seem to highlight and quantify the compression work penalty required for hydrogen pressurization for high pressure direct injection. This is arguably not an issue with the use of hydrogen in the engine but with its "production and storage". Very high hydrogen injection pressures also reduce considerably the amount of utilizable hydrogen from the full cylinder capacity to the final pressure (just higher than the injection pressure). The energy required for high pressure hydrogen compression is quantified in a later section of this paper. In this respect, the research presented in this work uses port injection as it provides the possibility to use hydrogen engines with readily available injectors.

Researchers are also studying the simultaneous combined combustion of fuels (one of which is hydrogen) to lower CO_2 emissions. Pukalskas [8] injected up to 30% energy content of hydrogen in a low-pressure (5 bar) port-injected SI gasoline engine. Shao [9] used a mixture of ammonia and hydrogen. Hydrogen was direct-injected at pressures ranging from 40 to 80 bar. Willens [6] used a diesel pilot injection to start the combustion of the hydrogen direct-injected fuel. Diesel fuel was injected at a rather low pressure of 290 bar, specifically stated to be 10 bar higher than the direct injection pressure of hydrogen at 280 bar to make sure no hydrogen goes back into the diesel system.

The emissions from hydrogen engines only exhibit NOx with no particulates and very little HydroCarbon (HC) resulting from the partial combustion of the lubricating oil. However, even NOx emissions go to very low values at lambda 2 and higher [2,10,11]. Measurements of NOx concentrations in the exhaust port from this research confirmed this finding and therefore these NOx results are not being replicated here.

The initial testing of the hydrogen engine performed by Portelli [12] was at stoichiometric conditions, λ = 1, and a switching EGO sensor was used to determine the stoichiometric mixture. This was done because the NGK #91101 wide band EGO sensor provided inaccurate readings during hydrogen operation. Additionally, it is widely accepted that abnormal combustion is expected in hydrogen stoichiometric mixtures. Subsequently, in this work, combustion characterization of hydrogen with λ = 2 and λ = 3 mixtures was per-

formed where precise measurement of the Mass Air Flow (MAF) was essential to determine the AFR.

This paper presents experimental results from the hydrogen operation of a 600 cc single cylinder engine at its nominal rotational speed (1250 rpm) and three load conditions (from part load, full load and slightly boosted). The combustion characteristics of hydrogen operation, i.e., the Mass Fraction Burned (MFB) history versus crank angle, was derived from the measured in-cylinder pressure, and the locations to reach 10, 50 and 90% of the combustion are given and discussed. Results from gasoline and propane operation are also presented for comparison purposes. Most importantly it was found that hydrogen produces a Brake Thermal Efficiency of 23% at λ = 3 Wide Open Throttle (WOT), compared to the 21% found from gasoline with stoichiometric conditions at WOT. As expected, gasoline at stoichiometric condition WOT had a higher Brake Mean Effective Pressure (BMEP) of 5.6 bar compared to hydrogen WOT operation where, at stoichiometric conditions, it had 3.5 bar and 2.6 bar at lambda 2.

Hydrogen heat loss to the cylinder wall has been researched by a number of researchers including Shudo, in a number of publications, Verhelst, Demuynck, Gürbüz, Wang and Beccari [4,10,11,13–20]. Demuynck placed a thermopile heat flux sensor on the cylinder wall while Gürbüz placed a fast response thermocouple. Researchers refer to the fact that hydrogen has a thinner quench layer compared to the traditional hydrocarbon fuel and hence the findings of augmented heat transfer to the wall during hydrogen operation is expected. Shudo made experiments at λ = 1 and at 50% volumetric efficiency, Demuynck made experiments at leaner mixtures, e.g., λ = 2, and Wang and Beccari tested higher λ values up to 3. Local heat flux measurements are very good to understand temporal behavior at discrete locations, however they lack the ability to give bulk heat transfer and also suffer from 2D and 3D effects and possibly fin effects [21,22]. Based on the thermopile heat flux sensor on a CFR engine operating at 600 rpm, Demuynck [19] found that hydrogen operation (at around λ = 2) has the highest maximum heat flux compared to gasoline, methanol and methane. However, in another publication, Demuynck [18] gave a heat flux history with a crank angle, and in [18], the hydrogen heat flux is lower and over a smaller crank angle compared to methane with both at λ = 1. Hence the claim that hydrogen has higher heat losses is doubtable. The heat loss can also be calculated from the difference between chemical fuel energy and apparent heat release [4,10,11,13–16]. Earlier hydrogen research focused more on stoichiometric operation [13–16] while the more recent studies moved to leaner operation [4,10,11].

Beccari [11] made a detailed numerical analysis based on an extensive experimental data set obtained on a CFR engine (at 900 rpm) in which the air-to-fuel ratio and Compression Ratio were varied. Unfortunately, the torque could not be measured on the CFR engine and hence the BMEP was not obtainable, therefore only Indicated Mean Effective Pressure (IMEP) values are given. Lambda was varied from 1.3 to 3.0 while the Compression Ratio was varied from 4.75 to 14.51. Beccari used the term Heat Loss Efficiency (HLE, which is the ratio of fuel chemical energy less the apparent heat released divided by the apparent heat released, hence less heat loss with a higher HLE) and showed that hydrogen at λ = 2 had a higher HLE than gasoline at λ = 1 and gasoline had a higher HLE than methane at λ = 1. Beccari also showed that HLE was unaffected by the Compression Ratio (CR).

In this study, the heat loss to the wall was analyzed from the difference between chemical heat and apparent heat release and also calculated from the chemical heat energy less the output mechanical energy and less the exhaust heat energy as detailed in a later section.

2. Methodology

The engine used to carry out tests using hydrogen fuel in this research was a single cylinder four stroke engine, the J.A.P. (England) Model 6 engine. The J.A.P. 6 engine is a stationary engine and was manufactured for industrial purposes [23]. The engine was designed to operate on gasoline. From the engine manual, the engine was described as having a power output of 5.5 brake horsepower (4.1 kW) at 1800 RPM. The engine details are given in Table 1.

Table 1. Engine specifications.

Engine Variable Measured	Value
Stroke	102.6 mm
Bore	86.1 mm
Engine Compression Ratio	5.36
Engine Swept Volume	597 cc
Inlet Valve Opens	17° before TDC
Inlet Valve Closes	52° after BDC
Exhaust Valve Opens	48° before BDC
Exhaust Valve Closes	9° after TDC

The engine is air-cooled by means of a fan that is integral to the flywheel, and the displaced air is deflected by the fan casing towards the fins of the cylinder head and cylinder block. The engine was braked by a Direct Current Plint and Partners (England) electrical dynamometer. Originally the engine was carbureted but was converted to electronic fuel injection. The full conversion to hydrogen operation and the safety aspects associated with using hydrogen leak detection sensors are detailed in Portelli [12].

2.1. LabVIEW Data Acquisition and Post-Processing

LabVIEW 2021 software was utilized to acquire and post-process the data recorded during testing. The aim of the research was to analyze the combustion characteristics of the SI engine whilst operating on gasoline, propane and hydrogen fuel injection. In-cylinder, crank angle-resolved pressure data was acquired along with other channels, namely: crank teeth, cam tooth, current through the spark ignition coil and current through the injector coil. The spark ignition coil current trace was used to measure the ignition delay and confirm the spark advance, while the injector current trace was used to confirm the DOI. The crank angle-resolved data is referred to here as the fast data to differentiate it from the slow data that was recorded at 10 Hz. The slow speed data at 10 Hz was also acquired using LabVIEW software to log slow speed parameters such as engine torque, mass air flow, exhaust gas temperature (1/16″ type K sheathed thermocouple), switching EGO sensor, NOx emissions, etc., which were measured directly by National Instruments DAQ. The slow speed DAQ also logged parameters from the ECU GUI data stream (by sniffing) such as engine speed, MAP, DOI and spark timing.

The pressure transducer, AVL (Graz, Austria) GH 13Z-24, integrated in the spark plug, was used to obtain the in-cylinder pressure and its output signal was fed to a charge amplifier (AVL (Graz, Austria) Flexifem Piezo Type 2P2G). TDC position was determined by using the motoring data and allowing for loss angle [24]. The in-cylinder pressure obtained from the piezo electric sensor was pegged to the MAP at bottom dead center (BDC). One hundred and fifty (150) cycles at each test point were used for the analysis. The fast data was acquired using a National Instruments PCI 6221 card and saved using TDMS

file format. The slow speed data was acquired using two NI USB 6009 modules and an RS232 link to the ECU and data saved in Comma Separated Values format.

2.2. Test Matrix and Procedure

The hydrogen test matrix, detailed in Table 2, lists all experiments that were conducted at a constant engine speed of 1250 RPM, which was chosen as it was the rpm that gave the best BMEP as detailed by Portelli [12]. The load was varied, i.e., MAP of 75, 95, and 120 kPa, across two different λ values (λ = 2 and λ = 3).

Table 2. Hydrogen test matrix with optimal spark timing for MBT at 1250 RPM, varying MAP and λ.

MAP (kPa)	λ	Spark Advance (° CA BTDC)
75	2	10
75	3	20
95	2	10
95	3	10
120	2	10
120	3	10

For comparison reasons, tests with propane and gasoline fuels at stoichiometric conditions were performed. For propane and gasoline fuels, MAP of 50 kPa was also possible but such fuels cannot operate at high lean mixtures as opposed to hydrogen, which supports operation at high lean conditions of λ = 2 and λ = 3. The propane and gasoline test matrix is listed in Table 3 since similar Maximum Brake Torque (MBT) timings were obtained for both fuels.

Table 3. Propane and gasoline test matrix with optimal spark timing for MBT at 1250 RPM, λ = 1 with varying MAP.

MAP (kPa)	λ	Spark Advance (CAD BTDC)
50	1	25
75	1	20
95	1	20

For each test condition, optimization of spark timing was done to achieve minimum spark timing for MBT conditions by performing spark advance sweeps. The resulting BMEP versus spark advance for the three tested fuels at 95 kPa is shown in Figure 1. The spark advance values in Tables 2 and 3 are the MBT values.

As shown in Figure 1, hydrogen exhibits a notably wider spark advance curve compared to gasoline and propane. For the traditional fuels, gasoline and propane, the MBT timing appears more pronounced from the characteristic shape of the curve, whereas for hydrogen, this distinction is less clear. Results show that the spark advance range between 10 and 0 Crank Angle Degrees (CADs) Before Top Dead Center (BTDC) tends to produce the maximum torque output and hence BMEP for hydrogen at the λ = 295 kPa condition. Literature reports from multiple sources [2,25,26] indicate that under similar operating conditions, SI was typically set between 10° and 15° CAD BTDC. The MBT timing for hydrogen at λ = 2 found in this research was 10° CAD BTDC. This optimal ignition advance is further examined and validated in later section in connection with the MFB50%.

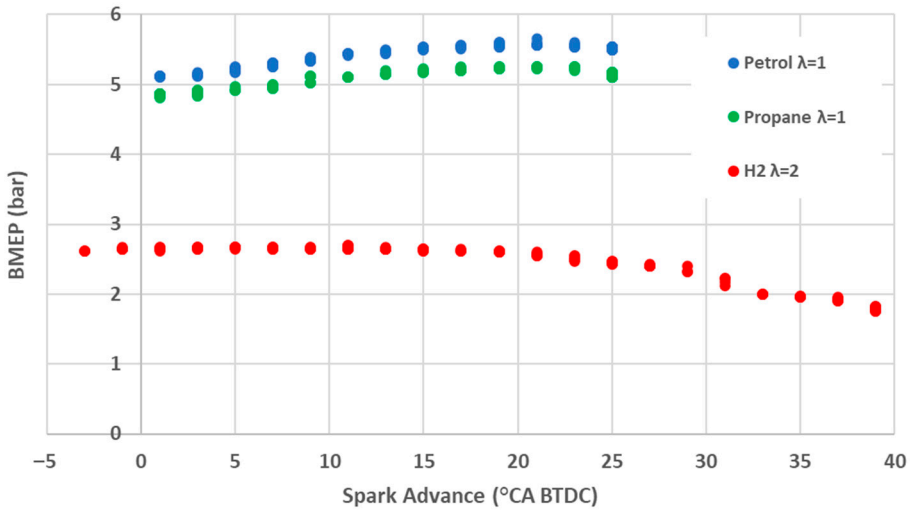

Figure 1. The spark sweeps (to determine MBT) performed for the three fuels at a MAP of 95 kPa.

2.3. Calculation of MEP Equivalent to Compress Hydrogen Gas

With shifts towards direct injection and higher injection pressures, consideration was given to the hydrogen pressurization penalty.

Hydrogen fuel is mainly stored in bottled high pressure form. Fully filled cylinders are at least at 200 bar (700 bar also mentioned) and therefore can supply pressures of 100 bar or 150 bar to the hydrogen injectors. However, if the injectors are operated at such high pressures, the usable quantity of hydrogen from the full quantity in the bottled hydrogen is reduced dramatically. If hypothetically we imagine that a compressor is used to fully consume the quantity of hydrogen in the bottles, the work required is considerable. Calculations were performed for compressor work and subsequently converted to equivalent MEP. A single-stage and a three-stage compression process (with complete intercooling in between stages), using a polytropic index of compression of 1.3, were considered for the calculations. The single-stage compressor was considered as it is the most basic form of compression that can be considered while the three-stage compression process was considered as it is a good compromise in complexity and efficiency as the highest efficiency is obtained with higher number of stages [27,28]. Heat loss in the compression process is handled by the polytropic index of 1.3 [27,28], however the mechanical efficiency of the drive to the compressor was not considered to simplify the calculation (i.e., 100% efficiency was considered but inclusion of a reasonable drive efficiency such as 95% can be easily integrated into the calculation). The results of this calculation are presented in Table 4.

Table 4. MEP equivalent of the work required to compress the hydrogen fuel at a boost of 2 bar absolute and lambda 2 operation.

Injection Pressure (bar)	MEP of Single-Stage Compressor (bar)	MEP of Three-Stage, Intercooled Compressor (bar)
3	0.53	0.47
10	1.29	1.04
35	2.35	1.69
70	3.07	2.08
100	3.50	2.29
150	4.02	2.53
200	4.42	2.71

For a reciprocating compressor, the work [J] required per second is

$$W_{comp} = \frac{n}{n-1}\dot{m}RT_1\left\{\left(\frac{p_2}{p_1}\right)^{(n-1)/n} - 1\right\}$$

where n is polytropic index of compression, $\dot{m}$ is the mass flow of hydrogen, R is the gas constant, T_1 is the upstream temperature, and p_2 and p_1 are the downstream and upstream pressures.

To find the MEP equivalent to compress the hydrogen required to operate an engine

$$\begin{aligned} MEP_{comp} &= \frac{W_{comp}}{V_{swept}} \\ &= \frac{n}{n-1} \times \frac{MAP \times R_{H_2}}{\lambda \times AFR_s \times R_{air}} \times \left\{\left(\frac{p_2}{p_1}\right)^{(n-1)/n} - 1\right\} \end{aligned} \quad (1)$$

where V_{swept} is the cylinder swept volume, R_{H2} is the hydrogen gas constant, AFR_s is stoichiometric AFR, λ is the ratio of actual AFR to AFR_s, and R_{air} is the air gas constant.

It is noted that for an engine that is boosted to 2 bar absolute and operated at lambda 2, the work required to compress the required hydrogen gas to 100 bar is equal to 2.3 bar MEP. This is quite a high MEP and is due to the high pressure requirement and the fact that hydrogen is a low density gas. Likewise, it is argued that if consideration is given to the loss of potential of work output when the hydrogen gas is expanded by a simple pressure regulator, this translates to a big waste. Therefore, expansion of the hydrogen in a proper expander could aid considerably in power output of the engine and reduce the exergy loss.

3. Experimental Results

The post-processing of the experimental data enabled combustion parameters to be studied. In subsequent graphs, the color code adopted for the three fuels is: blue for gasoline and green for propane, while hydrogen results are represented by red and orange for λ values of 2 and 3, respectively. Hydrogen results from earlier experiments [12] at λ = 1 are shown in dark red.

3.1. Brake Mean Effective Pressure

The BMEP was computed from the measured torque from the load cell and is shown in Figure 2. This figure shows a comparison for different fuels, and also for operation at different lambdas, which can be viewed as an unfair comparison, however the objective of this comparison is to get an overview and perspective of the end results in using these fuels at the most appropriate conditions for each respective fuel. As expected, the highest measured BMEP was with gasoline fuel at a MAP of 95 kPa (with a spark timing of 20° CA BTDC). The propane BMEP trend with MAP is similar to that of gasoline but slightly lower, as expected. This was expected as, although propane has a higher calorific value, the heating value of the air–fuel mixture is more important. Propane has a heating value for the mixture, which is 5% lower than gasoline mainly due to its density, and this normally produces a −5% performance. The observed lower BMEP for propane can also be explained by the lower MAF, resulting from the volumetric displacement caused by the injected propane vapor within the intake manifold. This directly affects the volumetric efficiency of the engine [29]. In a similar manner, hydrogen suffers in BMEP due to the fact that hydrogen displaces substantial portions of MAF.

Testing of hydrogen in λ = 1, λ = 2 and λ = 3 mixtures produced less torque (and consequently BMEP) when compared to the stoichiometric mixtures of propane and gasoline fuels. Despite performing boosted conditions of 120 kPa during hydrogen λ = 2 and λ = 3 testing, the maximum BMEP obtained during λ = 2 mixtures was approximately 20% lower

than that of gasoline. For the leaner λ = 3 mixture, hydrogen had a 40% lower BMEP than gasoline. Similar to propane, despite hydrogen having a higher calorific value, hydrogen displaces large amounts of air due to its low density. This shows the importance of boosting and direct injection after inlet valve closing as indicated by many researchers and discussed by Verhelst [30].

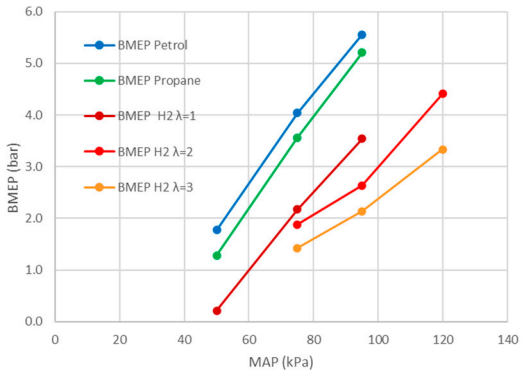

Figure 2. The variation of BMEP with variation in load represented by MAP for the three fuels.

3.2. Indicated Mean Effective Pressure

The in-cylinder pressure data was post-processed, and the IMEP was calculated and is shown in Figure 3. As expected, the characteristics of the IMEP curves presented in Figure 3 are similar to those of the BMEP depicted in Figure 2. The Friction Mean Effective Pressure (FMEP) was calculated as the difference between IMEP and BMEP and is shown in Figure 4 The values of FMEP are in the expected range but do show the inherent difficulty in the determination of FMEP as it is obtained by the subtraction of two much bigger values [31].

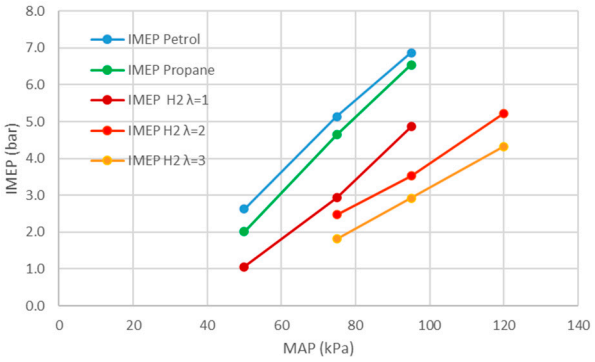

Figure 3. The variation of IMEP with variation in load represented by MAP.

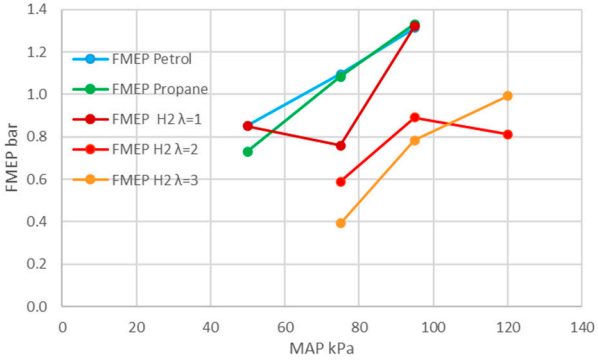

Figure 4. The variation of FMEP with variation in load represented by MAP.

3.3. Brake Thermal Efficiency

The variation of the Brake Thermal Efficiency (BTE) with different MAP values is presented in Figure 5. Comparing the BTE of the three fuels shown in Figure 5, hydrogen obtained the highest value of approximately 26% during both λ = 2 and λ = 3 mixtures, compared to 21% for gasoline and propane fuels. Limiting the comparison to the same MAP of 95 kPa, hydrogen has a slightly higher BTE of approximately 22% compared to that of gasoline (21%). Despite producing less torque (and hence BMEP) than gasoline and propane, hydrogen exhibited superior thermal efficiency. This indicates that hydrogen converts a greater proportion of the fuel's energy into mechanical work, suggesting a more thermodynamically efficient cycle and combustion process. This is likely due to its faster flame speed and hence is closer to constant volume heat addition [10,13–16,32]; however, heat losses also play a role and this is analyzed in a subsequent section.

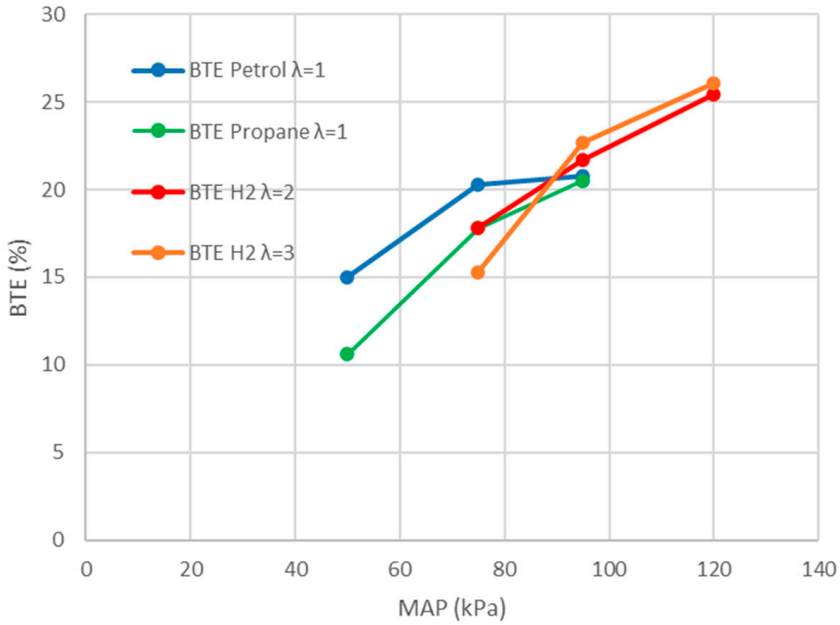

Figure 5. The variation of the BTE with variation in load represented by MAP.

3.4. In-Cylinder Pressure

The in-cylinder pressure curves for the three fuels at different MAPs are presented in Figure 6. By observing the shape characteristics of the in-cylinder pressure curves, several conclusions can be drawn. The most straightforward observation is that increasing the MAP results in higher in-cylinder pressures. As noted by Molina et al. [25] and Sementa et al. [2], during dilute conditions the curves widen and flatten due to low in-cylinder pressures, low bulk gas temperatures and longer burn durations. Additionally, the rate of pressure increase, which is due to the rate of heat release, is lower for leaner mixtures. As clearly indicated in all figures, gasoline exhibits the highest rate of heat release, a conclusion that is drawn on the steep gradients observed in the gasoline pressure curves.

Peak in-cylinder pressure values for all test conditions are given in Table A1 in Appendix A. The COV of the peak in-cylinder pressures is also given and shows that the variation in cycles is bigger in the λ = 3 compared to the λ = 2 condition. Other measured and derived values and their variations are given in Appendix A, Table A1, such as the measured torque and its variation.

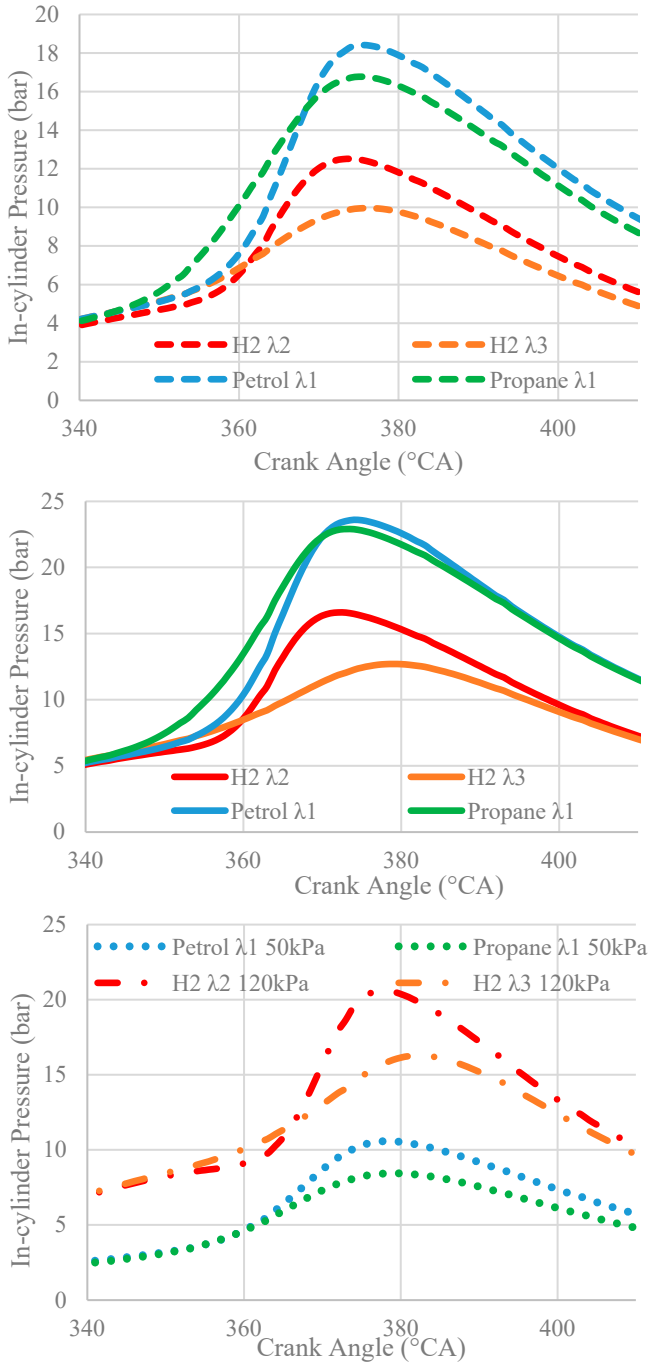

Figure 6. The variation of in-cylinder pressure with crank angle at a MAP of 75 kPa in upper plot, at a MAP of 95 kPa in middle plot and at MAPs of 50 kPa and 120 kPa in lower plot.

3.5. Mass Fraction Burned

The Mass Fraction Burned (MFB) profile was calculated following the widely known approach presented by Rassweiler and Withrow (and subsequently others) to obtain the MFB profiles [33–37].

$$MFB = x_b = \frac{p^{1/n}V - p_o^{1/n}V_o}{p_f^{1/n}V_f - p_o^{1/n}V_o} \quad (2)$$

The MFB profiles obtained showed that hydrogen is consistently faster in its burning profile compared to gasoline and propane and that hydrogen operation at λ = 2 is faster than hydrogen operation at λ = 3. The characteristics of the MFB, like MFB10% (CA10) and MFB50% (CA50), will be presented and discussed in a subsequent section.

3.6. Net Heat Release Rate

The net Heat Release Rate (HRR) was obtained by using Equation (3) [38] (Heywood 2nd edition, eqn 10.6). The peak net heat release rate is plotted in Figure 7.

$$\frac{dQ_{net}(\theta)}{d\theta} = \frac{\gamma}{\gamma - 1}.p(\theta).\frac{dV(\theta)}{d\theta} + \frac{1}{\gamma - 1}.V(\theta).\frac{dP(\theta)}{d\theta} \quad (3)$$

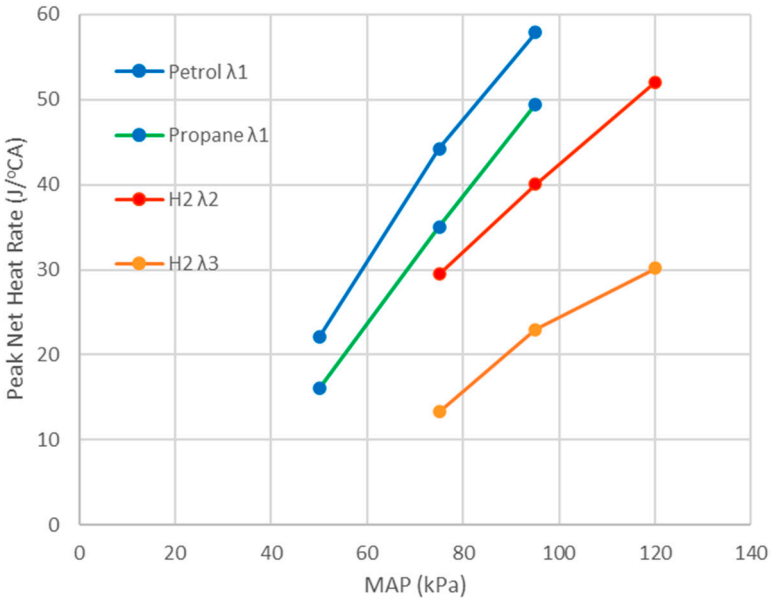

Figure 7. Variation of the peak net HRR with variation in load represented by MAP.

The highest peak HRR obtained was observed during gasoline testing where it developed the highest HRR of 58 J/°CA. This elevated HRR is one of the reasons for gasoline producing the highest torque. It is important to recognize that hydrogen appears to develop high peak HRRs compared to the torque it produced. This high peak HRR might be attributed to hydrogen's enhanced flame propagation, which accelerates combustion [39]. Ma et al. [40] argued that the peak HRR is influenced by the ignition timing, where a late spark timing improves the mixing time. Moreover, the late spark timing of 10 CAD BTDC used during hydrogen testing at a MAP of 95 kPa with a λ = 2 mixture might explain the observed high peak HRR. However, as deduced from the spark sweeps shown in Figure 7, later spark timings beyond the MBT timing of 10 CAD BTDC seem to have an insignificant effect on producing additional torque. This implies that torque is not solely determined by the peak HRR caused by the fuel but rather by the cumulative heat release as discussed in the following section.

3.7. Cumulative Heat Release Rate

The cumulative heat release for different MAP values is shown in Figure 8. It is widely accepted (J. B. Heywood [38], p. 859) that approximately 35% of the total energy fuel inputted in an internal combustion engine is converted into actual shaft or brake work. When friction was subtracted from the indicated work, similar percentage values were obtained showing that approximately 30% of the cumulative heat release is converted into usable torque. The plot shows a virtually linear cumulative heat release with the MAP for each fuel, which is due to the maintained λ. Furthermore, the plot shows that the cumulative heat release for gasoline is highest with hydrogen at λ = 3 being lowest, which is due to the fuel quantity being injected.

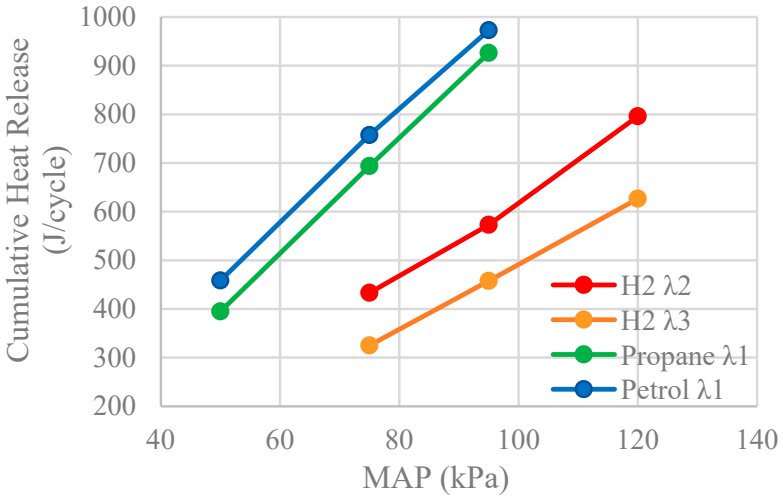

Figure 8. Variation of the cumulative heat release with variation in load represented by MAP.

3.8. MFB10%, MFB50% and MFB90% Locations

From the MFB profiles, the combustion locations MFB10%, MFB50% and MFB90% were determined. The MFB50% locations for all the fuels tested are shown in Figure 9.

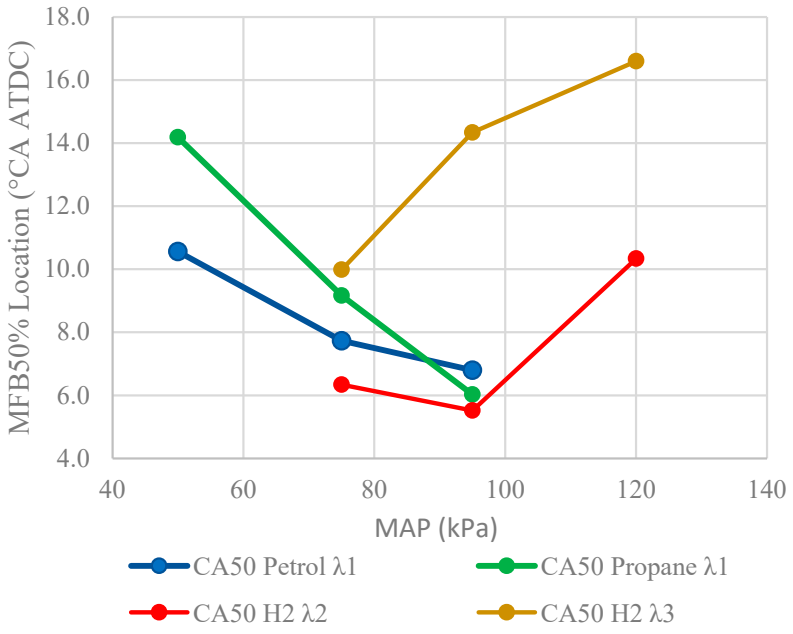

Figure 9. The variation of MFB50% locations with MAP using the Rassweiler and Withrow approach.

For traditional fuels, the main observation is that an increase in MAP corresponds to the MFB50% position occurring earlier with respect to TDC. When analyzing these combustion locations, it is important to consider the spark advance used, which, as shown in Table 3, was earlier only during the test with MAP 50 kPa. Moreover, although the same spark advance was used for MAPs of 75 kPa and 95 kPa, the resulting MFB50% positions differed due to the different heat release rate. Opposite behavior was noticed from the hydrogen analysis in both mixtures, where the MFB50% location appeared to occur later as the MAP increased. The MFB50% location for leaner mixtures occurred later due to the slower combustion rate. As an example, for the MAP test of 95 kPa, as shown in Table 2, for which the same ignition advance of 10 CAD BTDC was used for both $\lambda = 2$ and $\lambda = 3$, the MFB50% location was approximately equal to 6 CAD ATDC for $\lambda = 2$ while it was

approximately equal to 14 CAD ATDC for λ = 3. These MFB50% values align well with those reported by Sementa [2], who were also at WOT and who reported an MFB50% of 7.7 at λ = 2 and 11.64 at λ = 3, however, with a spark advance of 12.6 and 26.6 for λ = 2 and λ = 3, respectively. Comparisons were made with results obtained by Rrustemi et al. [26] who reported an MFB50% of 10 CAD ATDC at a MAP of 95 kPa for λ = 2 mixtures. At a MAP of 120 kPa and λ = 2 mixture, an MFB50% of 22 CAD ATDC was reported, which differs from the values obtained during this experimentation. Rrustemi et al. [26] did not perform investigations beyond λ = 2; therefore, comparisons for λ = 3 values cannot be made. Similarly, the MFB50% locations observed align closely with those reported by Molina et al. [25] during low load conditions.

As observed from Figure 1, the minimum spark ignition advance for MBT from the hydrogen curve appears less distinct compared to those for propane and gasoline fuels. Therefore, an exercise to analyze this behavior and the dependency of the engine output torque as a function of spark timing was done with reference to the MFB50% location. This helps to study the optimal position of the center of combustion (MFB50%) to produce the maximum net work output, thereby clearly identifying the optimum ignition advance. The MFB50% locations for spark sweeps of gasoline at λ = 1 and hydrogen at λ = 2 were obtained as shown in Figure 10.

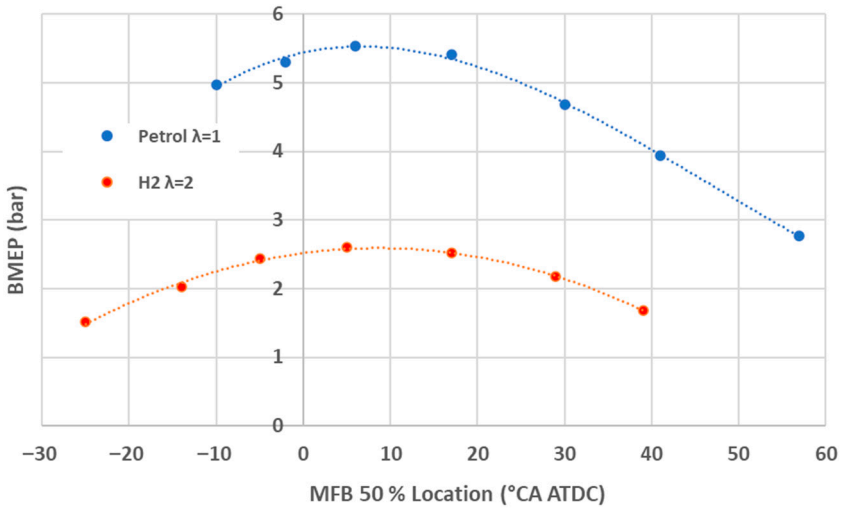

Figure 10. BMEP output against different MFB50% (CA50) locations.

As seen in Figure 10, the peak BMEP for both fuels occurred with MFB50% being later than the Top Dead Center (TDC). According to Beccari et al. [41], this shift occurs due to heat transfer between gas and cylinder walls and friction losses. Beccari et al. further explained that the primary cause of this shift is mainly due to heat losses while friction losses tend to have a smaller impact on this shift angle. As can be observed in Figure 10, the location of the MFB50% for the peak BMEP (net work output) for gasoline fuel deviated by approximately 7 CAD with respect to the TDC, which aligns well with the values suggested by J. B. Heywood ([38] p. 389) and Beccari [41]. For the hydrogen fuel, the peak net work output was obtained at an MFB50% location of approximately 10 CAD. This conclusion perfectly matches that obtained by Rrustemi et al. [26], Sementa et al. [2] and Molina et al. [25], who all obtained similar optimal MFB50% locations. Moreover, although H_2 has a higher burn rate compared to gasoline, the MFB50% position deviated further from the TDC than the MFB50% obtained during gasoline experiments. This was unexpected, as Beccari et al. [41] previously indicated that a faster burning charge typically reaches an optimal 50% MFB closer to the TDC than a slower burning mixture. However, it is important to note that the spark ignition advance was set to 20 CAD BTDC for gasoline, whereas it

was set to 10 CAD BTDC for hydrogen. Despite this, the MFB50% location did not differ significantly, further demonstrating hydrogen's faster burn duration. It can also be noted that the capability of using the MFB50% to represent the optimal combustion phasing, despite the great combustion speed difference, can also be used for a hydrogen engine.

The dependence of the best output with respect to heat losses on the MFB50% location, with the prevailing knowledge that hydrogen has bigger heat losses due to a thinner quench layer, prompted the investigation of heat loss analyses detailed in a later section.

The MFB10% and MFB90% locations are shown in Figure 11, where it can be noted that these MFB% locations remain relatively constant with the MAP. Additionally, from the MFB10% and MFB90% locations, the fast burn duration (MFB90%–MFB10%) was determined and discussed in the next section.

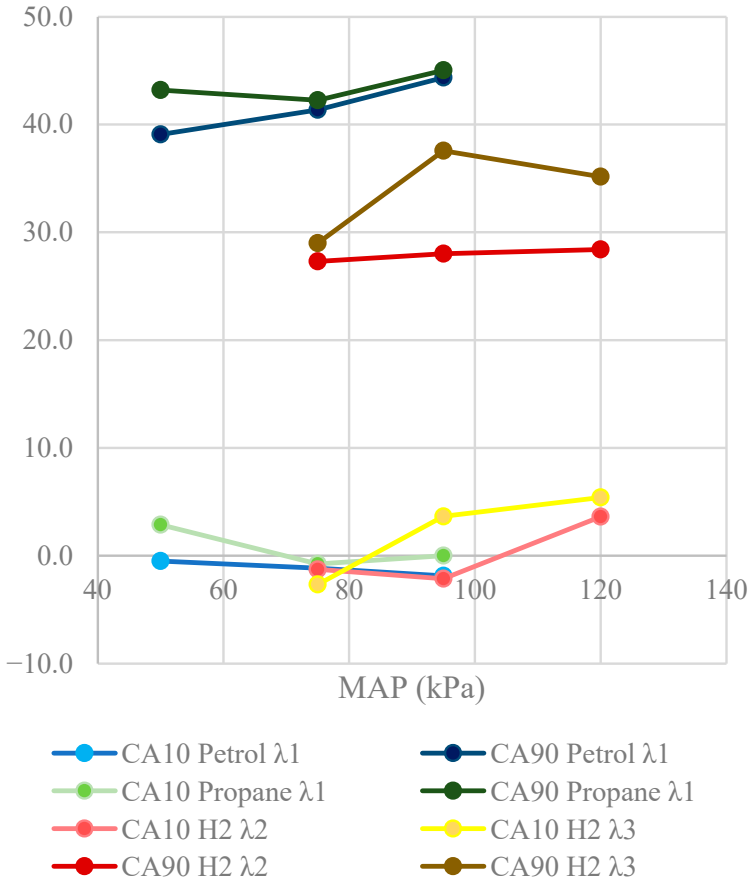

Figure 11. The variation of the MFB10% (CA10) and MFB90% (CA90) locations with variation in load represented by MAP.

3.9. Fast Burn Duration

The difference between the crank angle at MFB90% and the crank angle at MFB10%, referred to as the fast burn duration, for all fuels with respect to MAP is illustrated in Figure 12. The most notable distinction is the longer burn duration exhibited by traditional fuels compared to that observed during hydrogen testing. Additionally, the trends in the burn duration curves differ. While the burn duration of traditional fuels tends to increase with the MAP, hydrogen testing shows a negligible decrease in burn duration as the MAP increases. It is important to note that even at lean $\lambda = 3$ mixtures, hydrogen demonstrates a shorter burn duration than traditional fuels. Earlier research carried out by the authors at $\lambda = 1$ [12] showed a fast burn duration of just 7 CA. This is an important point to observe, as it is widely accepted that, under leaner mixture conditions, the flame speed tends to

decrease significantly, which is why earlier ignition advancement is typically required. These results highlight the rapid flame speed characteristic that hydrogen combustion possesses, a point which is emphasized by Al-Baghdadi [42].

Comparing these results to those reported by Negurescu et al. [43], shorter burn durations of 21 CAD at λ = 2 were reported, which align with those reported by Rrustemi [26]. This burn duration is slightly shorter than those depicted in Figure 12. For the λ = 3 mixture at Wide Open Throttle conditions (100 kPa), Negurescu et al. [43] reported a burn duration of 34 CAD ATDC, which is comparable to that depicted in Figure 12. For higher loads at λ = 2, Rrustemi et al. [26] reported a burn duration of approximately 29 CAD, which is slightly longer than that illustrated in Figure 12.

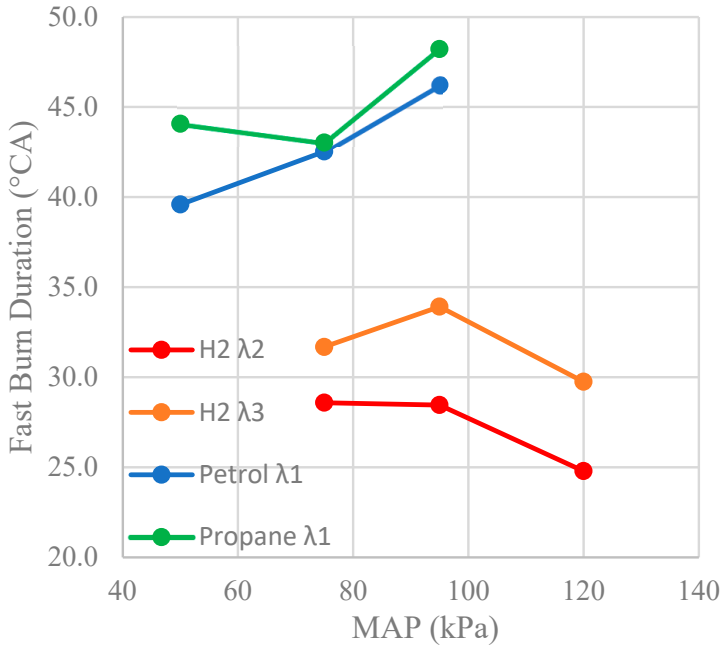

Figure 12. Comparison between the fast burn duration (CA90-CA10) evaluated for each fuel, MAP, and λ.

3.10. Ignition Delay

Figure 13 depicts the variation in ignition delay (i.e., the CA duration between the SI and the change in polarity of the HRR, where SI was determined as the point of drop in the spark ignition coil current in the fast data stream) with respect to the MAP. As expected, hydrogen λ = 3 mixtures exhibit a longer ignition delay compared to the richer λ = 2 mixture. The ignition delay for the hydrogen λ = 2 mixture remains relatively constant across the range of MAP values tested. In contrast, for the leaner λ = 3 mixture, the ignition delay shows a slight increase with increasing MAP. On the contrary, during both propane and gasoline testing, the ignition delay tends to decrease as the MAP increases. It is noted that the same spark plug, coil and coil ON time have been used in all the tests.

Since gasoline is injected in a liquid state, it would require time to vaporize. Despite this unavoidable time, it seems to have a lower ignition delay at lower MAP values compared to propane, which is injected in a vapor form. Thoo [44] comments on how the ignition delay is observed to be attributed to multiple factors such as the physical injection timing, mixing delay and chemical reaction delay. The author [44] observed similar characteristics to those mentioned by Obert [45] (pp. 297, 301) regarding results from performing gasoline testing where it is emphasized that with an increase in MAP, the ignition delay is decreased. This might take place since higher intake manifold pressures have a higher gas density, which cause higher in-cylinder temperatures during compression,

shortening the ignition delay. As commented by Hires et al. [46] the ignition delay is mostly affected by the ignition timing, where earlier timings cause higher ignition delays due to the low in-cylinder temperatures in the early compression phase.

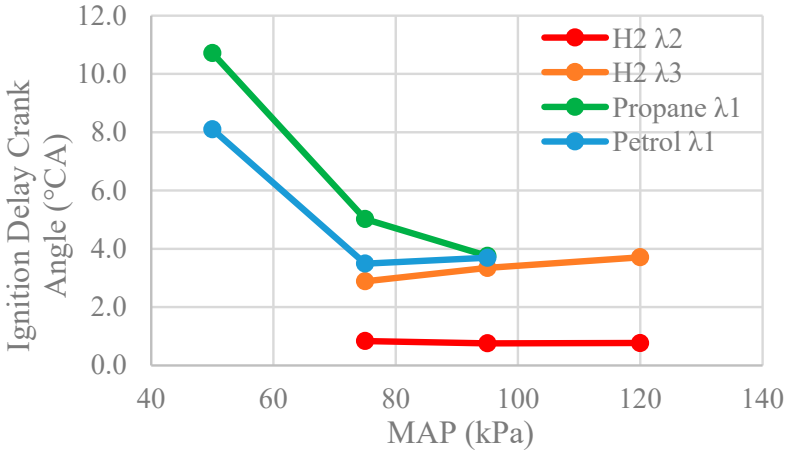

Figure 13. Variation of ignition delay with variation in load represented by MAP.

3.11. Energy Losses

The energy losses (E_L) were estimated through two approaches. The first approach was using Equation (4). The energy lost per Equation (4) primarily represents the heat lost; however, it also includes contributions from friction, blow-by gases and unburnt fuel, and auxiliary power (cooling fan, camshaft, etc.).

$$E_{L(4)} = \dot{m}_{fuel} LHV - \left(\dot{m}_{fuel} + \dot{m}_{air}\right) C_p (T_{ambient} - T_{exhaust}) - \frac{2\pi N\tau}{60} \quad (4)$$

The second approach is using Equation (5), which gives the energy lost as the fuel energy minus the net heat release into the gases.

$$E_{L(5)} = \dot{m}_{fuel} LHV - \sum_{i=ignition}^{i=end\ of\ combustion} \left(\frac{dQ_{net}(\theta)}{d\theta}\right)_i \quad (5)$$

As observed from Figure 14, similarities in the obtained values and curve characteristics were noticed. It is important to appreciate that the two approaches used contain information that was obtained differently, namely Equation (4) uses exhaust gas temperature and measured torque, while Equation (5) uses in-cylinder pressure. Therefore, the similarity in heat losses from both methods leads to a stronger observation that hydrogen has a lower heat loss than traditional fuels.

From Figure 14, for all the fuels with the increase in MAP, a higher heat loss was computed, which directly correlates to the higher in-cylinder combustion temperatures achieved from the higher pressures. This agrees with that reported by Demuynck et al., [19] who reported that heat flux reduced with the decrease in load (N.B. in [19], where the throttle angle is 90 at no load). Subsequently, the authors [19] commented on how the heat flux of hydrogen during lean mixtures seems to be equivalent to that reported during gasoline testing. In contrast, as observed in Figure 14, the heat losses of hydrogen during both mixtures tend to be less than those of gasoline. However, in their publication [18], when comparing methane and hydrogen operation, Demuynck showed distinctively that hydrogen heat flux to the wall is around ¼ of that of methane, and furthermore, the hydrogen heat flux history is over a much shorter crank angle when compared to methane operation.

It is also important to mention that the heat losses during the lean hydrogen λ = 3 mixture are less than those experienced during the richer hydrogen λ = 2 mixture due to the decrease in combustion temperature during the leaner mixture.

The heat loss determined from Equation (4) is dependent on $\dot{m}_{air}$ (mass flow of air measured as detailed in Appendix B), the determination of c_p as well as the measurement of the exhaust gas temperature. Exhaust gas temperature measurement was done with a 1/16 inch sheathed grounded thermocouple installed in the exhaust pipe at a plane with a 150 mm distance from the exhaust valve seat. It is accepted that a thermocouple measurement of exhaust gas temperature does not perfectly reflect the temperature of exhaust gases due to the issue of mass average versus time average measurements of temperature by the thermocouple, and the thermocouple is also affected by radiation effects [15]. Therefore, the heat loss determined through Equation (5) is more robust and will be discussed further.

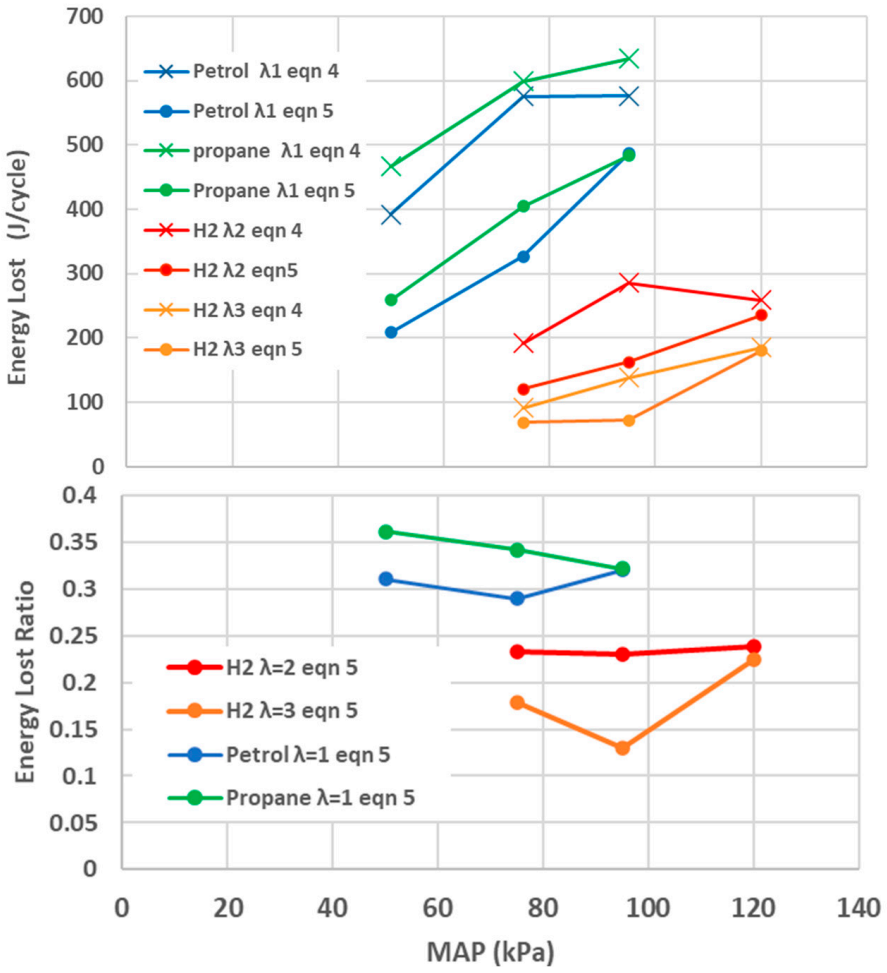

Figure 14. Upper chart: The variation of energy losses with MAP using the Equations (4) and (5) approach. Lower chart: Heat lost using Equation (5) as a ratio to the energy input with MAP.

The cumulative net heat released does not reach the value of the chemical energy of the fuel and the shortfall can be attributed to heat transfer and unburned fuel [38] (Heywood 2nd edition fig 9.14). It was observed that the highest cumulative net heat release values were obtained during hydrogen λ = 3 testing.

3.12. Energy Loss Ratio

To provide context and enable a better comparison, the calculated energy loss values were normalized by dividing the values by the total energy input (i.e., the multiplication of the mass of fuel and LHV) as depicted in the lower part of Figure 14. It can be seen that hydrogen heat loss (both heat transfer and unburned fuel) is lower than that of gasoline. As already mentioned, this is in contrast to the finding of Demuynck [19] (who noted that the heat flux of hydrogen during lean mixtures seems to be equivalent to that reported during gasoline testing). Therefore, this comparison through the energy loss ratio is an important observation and shows that the hydrogen operation and efficiency gain is not only due to faster combustion in itself.

4. Conclusions

Tests were carried out to investigate gasoline, propane and hydrogen combustion and the engine was operated successfully on hydrogen at λ = 2 and λ = 3.

A test matrix at MBT timings was determined, corresponding to 12 tests points for all three fuels: gasoline, propane and hydrogen. This was done after necessary spark sweeps were performed. It was observed that the burn duration of hydrogen at λ = 2 is 29 CAD compared to that of stoichiometric gasoline mixtures of 46 CAD. A shorter burn duration translates to a better Brake Thermal Efficiency of approximately 26% at λ = 3 mixtures. It was also noted that during hydrogen testing, the power output was lower than that during gasoline testing. This was mainly due to the lean hydrogen mixture used in comparison to the stoichiometric gasoline mixtures used. Additionally, when hydrogen is injected into the intake manifold, large amounts of air are displaced, significantly decreasing the volumetric efficiency of the engine. Moderate boosting to 120 kPa was aimed at reducing this shortfall in volumetric efficiency and hence in BMEP.

An analysis of the effect of the location of MFB50% on the BMEP was done. The optimal MFB50% position for gasoline was found to be 7 CAD ATDC and 10 CAD ATDC for hydrogen. It was concluded that, even for hydrogen operation, the capability of using the MFB50% to represent optimal combustion phasing (despite the great combustion speed difference compared to typical gasoline and propane fuels) can also be used for a hydrogen engine. That is, on a CFR engine where MBT cannot be determined, or in 1D engine simulations, the choice to impose an MFB50% around 8 CAD ATDC is a valid methodology even for hydrogen operation.

The energy losses (E_L) were estimated through two approaches. Great similarity was observed in the obtained values and curve characteristics from the two approaches. It is reiterated that the two approaches used contain information that was obtained differently, namely, Equation (4) uses exhaust gas temperature and measured torque while Equation (5) uses in-cylinder pressure. Therefore, the similarity in heat losses from both methods leads to a stronger observation that hydrogen has a lower heat loss than traditional fuels.

As expected, for all the fuels with an increase in MAP, a higher heat loss was computed, which directly correlates to the higher in-cylinder combustion temperatures achieved from the higher pressures. It was also noted that as expected, the heat losses during the lean hydrogen λ = 3 mixture are less than those experienced during the richer hydrogen λ = 2 mixture due to the decrease in combustion temperature during the leaner mixture.

Due to the dependence of Equation (4) on c_p as well as the exhaust gas temperature, it was noted that the heat loss determined through Equation (5) is more robust. It was also observed that the highest cumulative net heat release values were obtained during hydrogen λ = 3 testing.

For a better comparison, the calculated energy loss values were normalized by dividing the values by the total energy input. It was observed that the hydrogen heat loss ratio (both heat transfer and unburned fuel) is lower than that of gasoline.

Author Contributions: Conceptualization, E.P. and M.F.; Methodology, E.P. and M.F.; Software, A.F. and S.P.; Validation, A.F., S.P., E.P. and M.F.; Formal analysis, A.F., S.P. and M.F.; Investigation, A.F., S.P. and M.F.; Resources, M.F.; Data curation, A.F.; Writing—original draft, A.F.; Writing—review & editing, E.P. and M.F.; Supervision, E.P. and M.F.; Project administration, M.F.; Funding acquisition, M.F. All authors have read and agreed to the published version of the manuscript.

Funding: Project 'Palermo Malta Engine Research Networking' PalMal financed by Xjenza Malta through the Research Networking Scheme (RNS).

Data Availability Statement: The original contributions presented in the study are included in the article, further inquiries can be directed to the corresponding author.

Conflicts of Interest: The authors declare no conflict of interest.

Symbols and Abbreviations

The following abbreviations are used in this manuscript:

$A_{orifice}$	orifice area
A_t	throat area
c_D	coefficient of discharge
d_t	critical orifice diameter
E_L	Energy Losses
$\dot{m}_{air}$	mass airflow
m_{fuel}	mass of fuel
n	polytropic index of compression
p_0	upstream pressure
Q_{net}	net heat release rate
T_0	upstream temperature
ATDC	After Top Dead Center
BMEP	Brake Mean Effective Pressure
BTDC	Before Top Dead Center
BTE	Brake Thermal Efficiency
CA	Crank Angle
CAD	Crank Angle Degree
CR	Compression Ratio
DOI	Duration Of Injection
FMEP	Friction Mean Effective Pressure
GUI	Graphical User Interface
HC	Hydro Carbon
HLE	Heat Loss Efficiency
ICE	Internal Combustion Engine
IMEP	Indicated Mean Effective Pressure
MAF	Mass Air Flow
MAP	Manifold Absolute Pressure
MBT	Maximum Brake Torque
MEP	Mean Effective Pressure
MFB	Mass Fraction Burned
RPM	Revolutions Per Minute
TDC	Top Dead Center
WOT	Wide Open Throttle

Appendix A

Table A1. The mean and COV values of slow and fast data collected during the petrol, propane, hydrogen lambda2 and hydrogen lambda 3.

Load	Statistical Parameter	Measured Torque (Nm)	Work (J/Cycle)	Peak In-Cylinder Pressure (bar)	Peak Net HRR (J/CA)	Cumulative Net HRR (J/Cycle)	CA50 (CA ABDC)	Ignition Delay (CA)
Gasoline								
50 kPa	**Mean**	8.3	154.4	11.7	22.1	458.5	190.6	8.1
	COV (%)	0.8	1.3	3.7	8.7	1.0	1.3	19.7
75 kPa	**Mean**	18.9	302.0	19.8	44.2	757.6	187.7	3.5
	COV (%)	0.4	0.6	0.8	8.0	0.7	0.7	14.4
95k Pa	**Mean**	26	403.9	25.1	57.9	972.8	186.8	3.7
	COV (%)	2.3	0.6	1.8	7.7	0.7	0.7	12.5
Propane								
50k Pa	**Mean**	6.0	118.4	9.4	16.3	394.8	194.2	10.7
	COV (%)	1.9	16.3	15.6	21.4	7.7	3.8	34.7
75k Pa	**Mean**	16.7	273.2	17.9	36.5	693.7	189.2	5.0
	COV (%)	0.9	3.5	5.9	14.1	2.9	1.3	39.1
95 kPa	**Mean**	24.4	384.5	24.3	50.0	926.2	186.0	3.8
	COV (%)	2.3	1.6	3.1	10.2	1.7	0.9	24.8
H_2 λ2								
75 kPa	**Mean**	8.8	145.1	13.8	29.4	397.7	186.3	1.9
	COV (%)	0.8	1.7	2.3	8.5	2.0	1.0	50.5
95 kPa	**Mean**	12.4	207.5	18.1	40.0	522.3	185.5	1.4
	COV (%)	7.4	1.7	4.7	6.9	1.4	0.4	56.7
120 kPa	**Mean**	20.6	307.0	22.3	52.1	697.6	190.3	1.0
	COV (%)	2.3	1.2	3.0	7.1	1.0	3.0	55.3
H_2 λ3								
75 kPa	**Mean**	6.7	107.0	11.2	13.3	311.4	190	3.9
	COV (%)	2.9	8.3	4.7	13.9	6.2	4.1	64.0
95 kPa	**Mean**	10.0	171.8	14.3	23.4	457.7	194.3	3.3
	COV (%)	1.3	5.1	6.2	10.5	4.4	1.8	28.5
120 kPa	**Mean**	15.6	254.3	18.0	30.7	626.5	196.6	3.7
	COV (%)	0.7	2.5	5.4	8.2	2.2	1.4	17.1

High COV values indicate high cycle-to-cycle variations and indicate the combustion is not as stable.

Appendix B

Airflow Measurement Using Critical Flow Orifice

To determine the AFR during hydrogen testing, separate quantifications of the fuel and the air flow rates were performed. The fuel flow rate was determined through hydrogen flow tests of the injector performed using the volume collection method in the same manner as detailed in [38]. The air flow was determined through an installed critical flow orifice. This critical flow orifice utilizes chocked flow theory, which is ideal to measure pulsating air flow [47]. To create such a condition, compressed air was fed to the upstream of the critical flow orifice to maintain a higher pressure ratio than the downstream of the orifice at all times. These conditions allow the critical orifice to regulate the MAF through variations in the upstream pressure and orifice area, making it completely unaffected by changes in downstream pressure. Determination of the critical orifice diameter (d_t) was done through Equation (A1) [38].

$$\dot{m}_{air} = \frac{c_D A_t p_0}{\sqrt{RT_0}} \gamma^{\frac{1}{2}} \left(\frac{2}{\gamma + 1} \right)^{\frac{\gamma+1}{2(\gamma-1)}} \quad \text{(A1)}$$

And for the expected air flow of around 7.5 g/s,

$$d_t = 3.22 \times 10^{-3}\text{m} \approx 3\ \text{mm}$$

where A_t is the throat diameter, p_0 is the upstream pressure, T_0 is the upstream temperature, R is the air gas constant and the coefficient of discharge c_D = 0.982, according to the diameter ratio of 0.15 (β = d/D) [48].

Likewise, the hydrogen injector was also used in critical flow with an upstream pressure of 3.5 bar gauge. Sementa also commented that they used the injector in critical flow [2].

References

1. Arnold, E.R. Internal Combustion Engine Using Hydrogen as Fuel. London/England Patent 2183674, 19 December 1939.
2. Sementa, P.; Antolini, J.V.; Tornatore, C.; Catapano, F.; Vaglieco, B.M.; Sanchez, J.L.J. Exploring the potentials of lean-burn hydrogen SI engine compared to methane operation. *Int. J. Hydrogen Energy* **2022**, *47*, 25044–25056. [CrossRef]
3. Han, J.; Doosje, E.; Seykens, X.; Somers, L.M.T. Experimental study of H_2 injection strategies in a HD engine: Comparison of PFI and LPDI. *Int. J. Hydrogen Energy* **2025**, *178*, 151655. [CrossRef]
4. Wang, B.; Lin, H.; Bai, C.; Yang, C.; Chen, Y.; Zu, Z.; Yin, Y.; Cheng, X.; Li, Z. Combustion and heat transfer characteristics of a heavy-duty low-pressure-direct-injection hydrogen engine with a flat-roof-and-shallow-bowl combustion chamber. *Int. J. Hydrogen Energy* **2024**, *96*, 597–611. [CrossRef]
5. Wei, H.; Hu, Z.; Ma, J.; Ma, W.; Yuan, S.; Hu, Y.; Hu, K.; Zhou, L.; Wei, H. Experimental study of thermal efficiency and NOx emission of turbocharged direct injection hydrogen engine based on a high injection pressure. *Int. J. Hydrogen Energy* **2023**, *48*, 12905–12916. [CrossRef]
6. Willems, R.; Seykens, X.; Bekdemir, C.; Doosje, E.; Van Gompel, P. *The Potential of Hydrogen High Pressure Direct Injection Toward Future Emissions Compliance: Optimizing Engine-Out NOx and Thermal Efficiency*; SAE Technical Paper 2024-37-0005; SAE International: Warrendale, PA, USA, 2024. [CrossRef]
7. Ding, W.; Deng, R.; Deng, J.; Wang, C. Combustion characteristics optimization and thermal efficiency enhancement by stratified charge of hydrogen direct injection for argon power cycle hydrogen engine. *Int. J. Engine Res.* **2024**, *25*, 1461–1475. [CrossRef]
8. Pukalskas, S.; Rimkus, A.; Vipartas, T.; Stravinskas, S.; Kriaučiūnas, D.; Mejeras, G.; Ušinskas, A. Hydrogen Supplementation in SI Engines: Enhancing Efficiency and Reducing Emissions with a Focus on Knock Phenomena. *Machines* **2025**, *13*, 571. [CrossRef]
9. Shao, K.; Wu, H. Effect of Hydrogen Injection Strategy on Combustion and Emissions of Ammonia–Hydrogen Sustainable Engines. *Sustainability* **2025**, *17*, 9403. [CrossRef]
10. Beccari, S.; Pipitone, E.; Caltabellotta, S. Analysis of the Combustion Process in a Hydrogen-Fueled CFR Engine. *Energies* **2023**, *16*, 2351. [CrossRef]
11. Beccari, S.; Pipitone, E. Heat Transfer Modeling of Hydrogen-Fueled Spark Ignition Engine. *Energies* **2025**, *18*, 475. [CrossRef]
12. Portelli, S.; Farrugia, M. Mechatronics for Hydrogen Fuelling of Single Cylinder Internal Combustion Engine. In *Proceedings of the 20th International Conference on Mechatronics—Mechatronika (ME), Pilsen, Czech Republic*; IEEE: New York, NY, USA, 2022; pp. 1–7. [CrossRef]
13. Shudo, T.; Nakajima, Y.; Futakuchi, T. Thermal efficiency analysis in a hydrogen premixed combustion engine. *JSAE Rev.* **2000**, *21*, 177–182. [CrossRef]
14. Shudo, T.; Nabetani, S.; Nakajima, Y. Influence of specific heats on indicator diagram analysis in a hydrogen-fuelled SI engine. *JSAE Rev.* **2001**, *22*, 224–226. [CrossRef]
15. Shudo, T.; Suzuki, H. Applicability of heat transfer equations to hydrogen combustion. *JSAE Rev.* **2002**, *23*, 303–308. [CrossRef]
16. Shudo, T. Improving thermal efficiency by reducing cooling losses in hydrogen combustion engines. *Int. J. Hydrogen Energy* **2007**, *32*, 4285–4293. [CrossRef]
17. Verhelst, S.; Maesschalck, P.; Rombaut, N.; Sierens, R. Increasing the power output of hydrogen internal combustion engines by means of supercharging and exhaust gas recirculation. *Int. J. Hydrogen Energy* **2009**, *34*, 4406–4412. [CrossRef]
18. Demuynck, J.; Raes, N.; Zuliani, M.; De Paepe, M.; Sierens, R.; Verhelst, S. Local heat flux measurements in a hydrogen and methane spark ignition engine with a thermopile sensor. *Int. J. Hydrogen Energy* **2009**, *34*, 9857–9868. [CrossRef]
19. Demuynck, J.; De Paepe, M.; Verhaert, I.; Verhelst, S. Heat Loss Comparison Between Hydrogen, Methane, Gasoline and Methanol in a Spark-Ignition Internal Combustion Engine. *Energy Procedia* **2012**, *29*, 138–146. [CrossRef]
20. Gürbüz, H. Parametrical investigation of heat transfer with a fast response thermocouple in a SI engine. *J. Energy Eng.* **2016**, *142*, 04016014. [CrossRef]

21. Farrugia, M.; Alkidas, A.C.; Sangeorzan, B.P. Transient Surface Heat-Flux Measurements in the Exhaust of a SI Engine. *Intern. J. Veh. Des.* **2007**, *45*, 1–11. [CrossRef]
22. Caruana, C.; Farrugia, M.; Mollicone, P.; Pipitone, E.; Sammut, G. In-Cylinder Heat Transfer Determination Using Impulse Response Method with a Two Dimensional Characterization of the Eroding Surface Thermocouple. In *Proceedings of the 15th International Conference on Engines & Vehicles, Capri, Italy, 12–16 September 2021*; SAE Paper Number 2021-24-0018; SAE International: Warrendale, PA, USA, 2021. [CrossRef]
23. J.A.P. Models 4/2, 4/3, 5 & 6 Type 1 Industrial Engines General Description, Running and Maintenance, Instructions with Diagrams and Spare Parts List. Available online: http://staverlokk.no/jostein/motor/Dokument/JAP%20Models%204_2%204_3%205%206%20Type%201%20Reference%20Book%20&%20Spare%20Parts%20List.pdf (accessed on 28 November 2025).
24. Pipitone, E.; Beccari, A. Determination of TDC in internal combustion engines by a newly developed thermodynamic approach. *Appl. Therm. Eng.* **2010**, *30*, 1914–1926. [CrossRef]
25. Molina, S.; Novella, R.; Soriano, J.G.; Girona, M.O. Experimental Activities on a Hydrogen-Fueled Spark-Ignition Engine for Light-Duty Applications. *Energies* **2021**, *14*, 20.
26. Rrustemi, D.; Ganippa, L.; Axon, C. Investigation of boost pressure and spark timing on combustion and NO emissions under lean mixture operation in hydrogen engines. *Fuel* **2023**, *353*, 129192. [CrossRef]
27. Eastop, T.D.; McConkey, A. *Applied Thermodynamics for Engineering Technologists*; Longman: London, UK, 1993.
28. Moran, M.J.; Shapiro, H.N.; Boettner, D.D.; Bailey, M.B. *Fundamentals of Engineering Thermodynamics*; John Wiley & Sons: New York, NY, USA, 2014.
29. Farrugia, M.; Briffa, A. *Liquid State LPG Conversion of an Older Vehicle*; SAE Technical Paper 2014-01-2613; SAE International: Warrendale, PA, USA, 2014.
30. Verhelst, S.; Wallner, T. Hydrogen-fueled internal combustion engines. *Prog. Energy Combust. Sci.* **2009**, *35*, 490–527. [CrossRef]
31. Caruana, C.; Farrugia, M.; Sammut, G.; Pipitone, E. Further Experimental Investigation of Motored Engine Friction Using Shunt Pipe Method. SAE technical Paper 2019-01-0930. *SAE Int. J. Adv. Curr. Pract. Mobil.* **2019**, *1*, 1444–1453. [CrossRef]
32. Purayil, S.T.P.; Al-Omari, S.A.B.; Elnajjar, E. Experimental investigation of spark timing on extension of hydrogen knock limit and performance of a hydrogen-gasoline dual-fuel engine. *Int. J. Hydrogen Energy* **2024**, *49*, 910–922.
33. Rassweiler, G.M.; Withrow, L. Motion Pictures of Engine Flames Correlated with Pressure Cards. *SAE Trans.* **1938**, *33*, 185–204.
34. Amann, C.A. Cylinder-Pressure Measurement and Its Use in Engine Research. *SAE Trans.* **1985**, *94*, 418–435.
35. Stone, C.R.; Green-Armytage, D.I. Comparison of Methods for the Calculation of Mass Fraction Burnt from Engine Pressure—Time Diagrams. *Proc. Inst. Mech. Eng. Part D Transp. Eng.* **1987**, *201*, 61–67. [CrossRef]
36. Brunt, M.F.; Rai, H.; Emtage, A.L. The Calculation of Heat Release Energy from Engine Cylinder Pressure Data. *SAE Trans.* **1998**, *107*, 1596–1609.
37. Ball, J.K.; Raine, R.R.; Stone, C.R. Combustion analysis and cycle-by-cycle variations in spark ignition engine combustion Part 1: An evaluation of combustion analysis routines by reference to model data. *Proc. Inst. Mech. Eng. Part D J. Automob. Eng.* **1998**, *212*, 507–523.
38. Heywood, J.B. SI Engine Fuel Metering and Manifold Phenomena. In *Internal Combustion Engine Fundamentals*; McGraw Hill Inc.: Columbus, OH, USA, 1988.
39. Ghazal, H.O. Combustion analysis of hydrogen-diesel dual fuel engine with water injection technique. *Case Stud. Therm. Eng.* **2019**, *13*, 100380. [CrossRef]
40. Ma, F.; Yang, W.; Xu, J.; Li, Y.; Zhao, Z.; Zhang, Z.; Wang, Y. Experimental Investigation of Combustion Characteristics on Opposed Piston Two-Stroke Gasoline Direct Injection Engine. *Energies* **2021**, *14*, 2105. [CrossRef]
41. Beccari, A.; Beccari, S.; Pipitone, E. An Analytical Approach for the Evaluation of the Optimal Combustion Phase in Spark Ignition Engines. *J. Eng. Gas Turbines Power* **2018**, *132*, 032802. [CrossRef]
42. Al-Baghdadi, M.S. Effect of compression ratio, equivalence ratio and engine speed on the performance and emission characteristics of a spark ignition engine using hydrogen as a fuel. *Renew. Energy* **2004**, *29*, 2245–2260. [CrossRef]
43. Negurescu, N.; Pana, C.; Cernat, A. Aspects of using hydrogen in SI engine. *UPB Sci. Bull. Ser. D Mech. Eng.* **2012**, *74*, 11–20.
44. Thoo, W.J. A Study of the Ignition Delay Characteristics of Combustion in a Compression Ignition Engine Operating on Blended Mixtures of Diesel and Gasoline. Ph.D. Thesis, The University of Nottingham, Malaysia Campus, Semenyih, Malaysia, 2016.
45. Obert, E. *Internal Combustion Engines*, 3rd ed.; International Textbook Company: Scranton, PA, USA, 1968.
46. Hires, S.; Tabaczynski, R.; Novak, J. *The Prediction of Ignition Delay and Combustion Intervals for a Homogeneous Carge, Spark Ignition Engine*; SAE Technical Paper 780232; SAE International: Warrendale, PA, USA, 1978.

47. Kastner, L.J.; Williams, T.; Sowden, R. Critical-Flow Nozzle Meter and its Application to the Measurement of Mass Flow rate in Steady and Pulsating Streams of Gas. *J. Mechnical Eng. Sci.* **1964**, *6*, 88–98. [CrossRef]
48. *ISO 5167-3*; Measurement of Fluid Flow by Means of Pressure Differential Devices Inserted in Circular-Cross Section Conduits Running Full. International Organization for Standardization: Geneva, Switzerland, 2003.